Technical Article

TEAM Workshop Problem No. 10 revisited: extension to sinusoidal voltage excitation

***Abstract* — A modification of TEAM Workshop Problem No. 10 featuring a sinusoidal voltage excitation of the coil is treated by various finite element techniques with the aim of obtaining the steady-state periodic solution. The resulting nonlinear eddy current problem is formulated in terms of a current vector potential T and a magnetic scalar potential Φ. The time-stepping method practically reaching steady-state over many periods is used to yield a reference solution. This is compared to results obtained by a time-harmonic approximation as well as by a time domain method yielding the non-sinusoidal steady-state directly. The superiority of this latter technique is demonstrated.**

I. Introduction

Applying the method of finite elements (FEM) to nonlinear electromagnetic field problems leads to a system of nonlinear ordinary differential equations in time. The most straightforward method to solve this system is time-stepping (*TS*) requiring the solution of a large nonlinear algebraic equation system at each time step. This can be very time consuming, especially in case of three-dimensional problems. If the excitations are non-periodic or if, in case of periodic excitations, the transient solution is required, one cannot avoid time-stepping. In many cases however, the excitations of the problem are periodic, and it is only the steady-state periodic solution which is needed. Then, it is wasteful to step through several periods to achieve this by the "brute force" method [1] of time stepping.

If the excitation is sinusoidal, the simplest method is to make use of the crude approximation assuming that all quantities are sinusoidal as well, but to take account of the nonlinear relationship between the flux density and the magnetic field intensity, see e.g. [2] and [3]. This will be referred to as nonlinear time harmonic (*NTH*) method in the following.

A method known from the literature to avoid stepping through several periods in such a case is the time-periodic finite element method introduced in [4]. To accelerate the originally slow convergence of the method, a singular-decomposition technique has been introduced in [5] and it has even been parallelised in [6].

A new time domain technique using the fixed-point method to decouple the time steps has been introduced in [7] and applied to two-dimensional eddy current problems described by a single component vector potential. The optimal choice of the fixed-point permeability for such problems has been presented in [8] both in the time domain and using harmonic balance principles. The application of the method to three-dimensional problems in terms of a magnetic vector potential and an electric scalar potential as well as employing a current vector potential and a magnetic scalar potential has been described in detail in [9]. In contrast to the time-periodic finite element method, the periodicity condition is directly present in the formulation instead of being satisfied iteratively. This technique will be referred to as time-domain fixed-point (*TDFP*) method in what follows.

The aim of this work is to illustrate the advantages of the *TDFP* method using a modified version of TEAM Problem No. 10 [10] with the exponential current excitation of the coil being replaced by a sinusoidal voltage excitation.

The paper is structured as follows: In the following section II, TEAM Problem No. 10 is briefly reviewed and the modifications taken are explained. The methods used are described in section III with one sub-section devoted to the *TS*, the *NTH* and the *TDFP* methods each. In Section IV, the numerical results are presented and compared. The results of the paper are concluded in section V.

II. TEAM Problem No. 10

TEAM Problem No. 10 was put forward as early as 1988 at one of the first TEAM (Testing Electromagnetic Analysis Methods) Workshops at Argonne [11] by the group of T. Nakata of the Okayama University, Japan. The final definition along with numerical results by many groups from all over the world as well as measured values was then established in [10]. The present problem definition is taken from there.

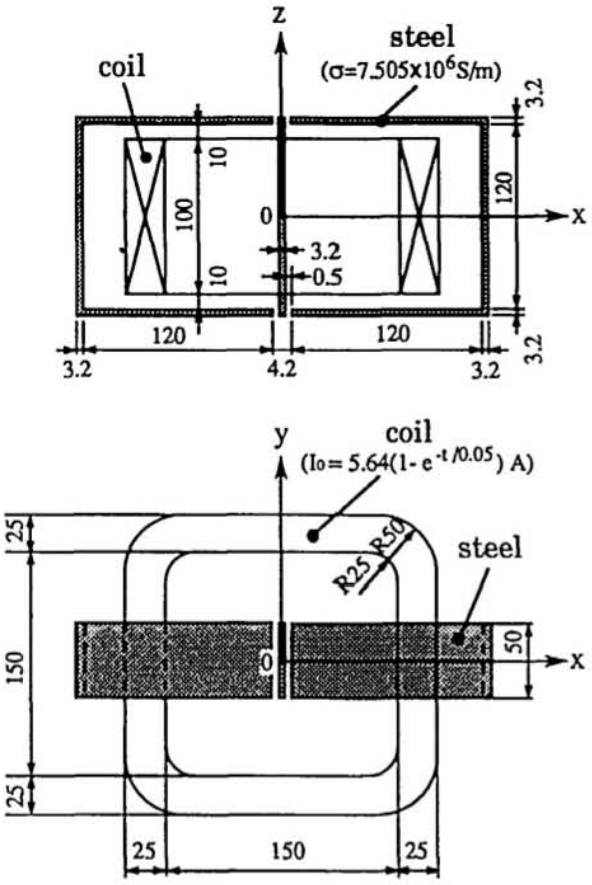

Fig. 1. Geometry of TEAM Problem No. 10

The geometrical dimensions are shown in Fig. 1. The steel plates are made of ferromagnetic material with its conductivity given as $\sigma = 7.505\text{x}10^6$ *S/m* in Fig. 1 as well, and

its nonlinear *B-H* curve shown in Table I for flux density values up to 1.8 *T* (**B** is flux density and **H** is magnetic field intensity).

TABLE I. B-H CURVE OF THE STEEL PLATE

No.	*B*(*T*)	*H*(*A/m*)	No.	*B*(*T*)	*H*(*A/m*)
1	0	0	15	0.90	313
2	0.0025	16	16	1.00	342
3	0.0050	30	17	1.10	377
4	0.0125	54	18	1.20	433
5	0.025	93	19	1.30	509
6	0.05	143	20	1.40	648
7	0.10	191	21	1.50	933
8	0.20	210	22	1.55	1228
9	0.30	222	23	1.60	1934
10	0.40	233	24	1.65	2913
11	0.50	247	25	1.70	4993
12	0.60	258	26	1.75	7189
13	0.70	272	27	1.80	9423
14	0.80	289			

For higher flux densities it is approximated as

$$B = \begin{cases} \mu_0 H + \left(aH^2 + bH + c\right) & \left(1.8T \le B \le 2.22T\right) \\ \mu_0 H + M_s & \left(B \ge 2.22T\right) \end{cases} \quad (1)$$

where a = -2.381x10^{-10}, b = 2.327x10^{-5}, c = 1.590, M_s =2.16 *T*. The number of turns in the coil is 162.

In the original definition of the problem, the current of the coil was defined as starting from zero at $t = 0$ and exponentially approaching a constant value as indicated in Fig. 1. Obviously, such a current form can be achieved by switching a constant voltage to the unenergised coil at $t = 0$. However, this non-periodical excitation does not well serve the purposes of the paper.

Therefore, a time-harmonic voltage $u(t)$ is assumed to be switched to the unenergised coil at $t = 0$ with the voltage starting from zero, i.e. it is described by a sine function:

$$u(t) = \hat{U}\sin\left(\omega t\right). \quad (2)$$

Selecting the frequency $f = \omega/2\pi$ to be 50 *Hz*, leads to a penetration depth of less than one millimetre with the maximal permeability μ corresponding to the *B-H* curve of Table I. Hence, appreciable skin effect can be anticipated in the plates.

The transients to be expected are governed by the resistance of the coil. If this were chosen very low, the TS method would be totally unfeasible for solving the problem, since it would require too many periods to step through before reaching steady-state. Targeting a time constant around the value of 50 *ms* (as in the original definition of the problem, see Fig. 1), means that twenty periods of time stepping (400 *ms*) should lead to near steady-state. In order to achieve this, a linear, static version of the problem has been solved using the relative permeability of $\mu_r = 2327$ corresponding to the point at $B = 1$ *T* of the *B-H* curve. To get the inductance of the coil, its flux linkage λ is computed from the well-known formula

$$\lambda = \frac{1}{i}\int_\Omega \mathbf{A}\cdot\mathbf{J}_0 d\Omega \quad (3)$$

where Ω is the problem domain, i the coil current, **A** is a magnetic vector potential fulfilling $\mathbf{B} = curl\mathbf{A}$ and $\mathbf{J}_0$ is the given current density of the coil. Introducing the current vector potential $\mathbf{t}_0$ corresponding to a unit coil current, i.e. satisfying

$$\mathbf{J}_0 = icurl\mathbf{t}_0, \quad (4)$$

(3) can be rewritten as

$$\lambda = \int_\Omega \mathbf{A}\cdot curl\mathbf{t}_0 d\Omega = \int_\Omega curl\mathbf{A}\cdot\mathbf{t}_0 d\Omega + \oint_{\partial\Omega}\left(\mathbf{t}_0\times\mathbf{A}\right)\cdot\mathbf{n}d\Gamma \quad (5)$$

where $\partial\Omega$ is the boundary of Ω. The integrand of the surface integral vanishes on symmetry planes and also on far boundaries where the tangential component of $\mathbf{t}_0$ can be assumed to be zero, therefore, the surface integral in (5) can be disregarded leading to

$$\lambda = \int_\Omega \mathbf{B}\cdot\mathbf{t}_0 d\Omega. \quad (6)$$

Note that (6) is valid for any potential formulation and also in the nonlinear case.

Dividing the flux linkage by the current yields the inductance arriving at a value of about $L = 18$ *mH*. To get a time constant of 50 *ms*, the resistance is chosen as $R = 0.36$ Ω. The amplitude $\hat{U}$ of the voltage in (2) is selected so that, in the linear case, the amplitude of the current should be about the same as in the steady-state value of the original problem definition ($\hat{I} = 5.64$ *A*, see Fig. 1). Since $\omega L \gg R$, this results in $\hat{U} \approx \omega L\hat{I} \approx 32$ *V*. In order to increase the saturation of the plates and hence to make nonlinearity more pronounced, computations with a voltage amplitude of 64 *V* have also been carried out. In summary, the data of the modified problem are summarized in Table II.

TABLE II. DATA OF THE MODIFIED PROBLEM

Voltage amplitude	$\hat{U}_1$	32 *V*
	$\hat{U}_2$	64 *V*
Frequency	$f = \frac{\omega}{2\pi}$	50 *Hz*
Coil resistance	R	0.36 Ω

III. METHODS

The potential formulation used is in terms of a current vector potential **T** and a magnetic scalar potential Φ. The current density of the coil is described by the current vector potential $\mathbf{t}_0$ introduced in (4). The function $\mathbf{t}_0$ is constructed to have a *z*-component only with a constant value in the hole of the coil, being zero outside the coil everywhere else and varying linearly within the coil [12]. The magnetic field intensity **H** is expressed by the potentials as

$$\mathbf{H} = i\mathbf{t}_0 - grad\Phi \qquad \text{in } \Omega_n, \quad (7)$$

$$\mathbf{H} = i\mathbf{t}_0 + \mathbf{T} - grad\Phi \qquad \text{in } \Omega_c \quad (8)$$

where i is the coil current, Ω_n is the eddy current free region made up by the air and the coil and Ω_c is the eddy current region constituted by the steel plates. The eddy current density in Ω_c is written as

$$\mathbf{J} = curl\mathbf{T} \quad \text{in } \Omega_c, \tag{9}$$

since the *curl* of $\mathbf{t}_0$ vanishes in Ω_c.

Maxwell's equations to be solved are

$$div\mathbf{B} = 0 \quad \text{in } \Omega_n \text{ and } \Omega_c \tag{10}$$

and

$$curl\mathbf{E} = -\frac{\partial \mathbf{B}}{\partial t} \quad \text{in } \Omega_c \tag{11}$$

where **E** is the electric field intensity.

Taking account of the constitutive relationships

$$\mathbf{B} = \mu\left(|\mathbf{H}|\right)\mathbf{H} \tag{12}$$

and

$$\mathbf{J} = \sigma\mathbf{E}\,, \tag{13}$$

the differential equations to be solved are hence

$$div\mu\left(i\mathbf{t}_0 - grad\Phi\right) = 0 \quad \text{in } \Omega_n \tag{14}$$

and

$$curl\left(\frac{1}{\sigma}curl\mathbf{T}\right) + \frac{\partial}{\partial t}\mu\left(i\mathbf{t}_0 + \mathbf{T} - grad\Phi\right) = 0 \text{ in } \Omega_c, \tag{15}$$

$$div\mu\left(i\mathbf{t}_0 + \mathbf{T} - grad\Phi\right) = 0 \quad \text{in } \Omega_c. \tag{16}$$

The given voltage of the coil is the sum of the voltages of the coil resistance and inductance. The former one is Ri and the latter one is the time derivative of the flux linkage λ. Using (6), this yields the additional equation

$$Ri + \int_{\Omega} \frac{\partial \mathbf{B}}{\partial t} \cdot \mathbf{t}_0 d\Omega = u\,. \tag{17}$$

The numerical solution of the problem is carried out by the method of finite elements using different techniques to solve the system of ordinary differential equations arising.

A. Time stepping method

Introducing the edge based vector basis functions $\mathbf{N}_i(\boldsymbol{r})$ (i = 1, 2, ..., n_e) and the node based scalar basis functions $N_i(\boldsymbol{r})$ (i = 1, 2, ..., n_n) in the finite elements (n_e is the number of edges, n_n the number of nodes in the finite element mesh, $\boldsymbol{r}$ denotes the space coordinates), the potentials are approximated as

$$\mathbf{T}\left(\mathbf{r},t\right) \approx \mathbf{T}_h\left(\mathbf{r},t\right) = \sum_{k=1}^{n_e} t_k\left(t\right)\mathbf{N}_k\left(\mathbf{r}\right), \tag{18}$$

$$\Phi\left(\mathbf{r},t\right) \approx \Phi_h\left(\mathbf{r},t\right) = \sum_{k=1}^{n_n} \phi_k\left(t\right)N_k\left(\mathbf{r}\right). \tag{19}$$

The vector $\mathbf{t}_0$ is represented by edge basis functions similarly to **T** in (18). The coefficients for $\mathbf{t}_0$ are easily computed as its line integrals along the edges of the finite element mesh. **T** is zero in Ω_n, i.e. all its degrees of freedom are set to zero in this region and also on its boundary. Hence, the tangential component of **T** is zero on the interface between Ω_n and Ω_c.

Galerkin's method with the weighting functions $\mathbf{N}_i(\mathbf{r})$ is applied to (15) and with the weighting functions $N_i(\mathbf{r})$ to the time derivative of (14), (16) assuming boundary conditions either specifying the normal component of **B** or the tangential component of **H** to vanish on the boundary ($\mathbf{B}.\mathbf{n} = 0$ or $\mathbf{H} \times \mathbf{n} = 0$). The resulting ordinary differential equations are appended by (17) with **B** expressed using (12), (7) and (8) and employing the approximations (18), (19) for the potentials. The resulting equations have a symmetric form:

$$\int_{\Omega_c} curl\mathbf{N}_i \cdot \frac{1}{\sigma} curl\mathbf{T}_h d\Omega + \frac{d}{dt}\int_{\Omega_c} \mu\mathbf{N}_i \cdot \left(\mathbf{T}_h - grad\Phi_h\right) d\Omega + \frac{di}{dt}\int_{\Omega_c} \mu\mathbf{N}_i \cdot \mathbf{t}_0 d\Omega = 0\,, \quad i=1, 2, ..., n_e, \tag{20}$$

$$-\frac{d}{dt}\int_{\Omega_n+\Omega_c} \mu gradN_i \cdot \left(\mathbf{T}_h - grad\Phi_h\right) d\Omega - \frac{di}{dt}\int_{\Omega_n+\Omega_c} \mu gradN_i \cdot \boldsymbol{t}_0 d\Omega = 0\,, \quad i=1, 2, ..., n_n, \tag{21}$$

$$\frac{d}{dt}\int_{\Omega_n+\Omega_c} \mathbf{t}_0 \cdot \mu\left(\mathbf{T}_h - grad\Phi_h\right) d\Omega + Ri + \frac{di}{dt}\int_{\Omega_n+\Omega_c} \boldsymbol{t}_0 \cdot \mu\mathbf{t}_0 d\Omega = u\,. \tag{22}$$

Gathering the unknown time functions $t_k(t)$ (k = 1, 2, ..., n_e) and $\phi_k(t)$ (k = 1, 2, ..., n_n) in (18) and (19) as well as the unknown current $i(t)$ in a vector $\mathbf{x}(t)$, the matrix form of (20), (21), (22) is the system of ordinary differential equations

$$\mathbf{S}\mathbf{x}\left(t\right) + \frac{d}{dt}\left[\mathbf{M}\left(\mu\left(\mathbf{x}\left(t\right)\right)\right)\mathbf{x}\left(t\right)\right] = \mathbf{f}\left(t\right) \tag{23}$$

where the stiffness matrix **S** is independent of **x** and hence of time, but the mass matrix **M** depends on the permeability which is itself field- and time-dependent. The right hand side vector is denoted by **f**. In our case, **f** satisfies the periodicity condition $\mathbf{f}(t) = \mathbf{f}(t+T)$ where T is the period $1/f$. The product of the mass matrix and the unknown vector is differentiated with respect to time.

The vectors **x** and **f** as well as the matrices **S** and **M** are partitioned as

$$\mathbf{x} = \begin{Bmatrix} \mathbf{x}^T \\ \mathbf{x}^\Phi \\ i \end{Bmatrix}, \tag{24}$$

$$\mathbf{f} = \begin{Bmatrix} \mathbf{0} \\ \mathbf{0} \\ u \end{Bmatrix}, \tag{25}$$

$$\mathbf{S} = \begin{bmatrix} \mathbf{S}^{TT} & \mathbf{0} & \mathbf{0} \\ \mathbf{0} & \mathbf{0} & \mathbf{0} \\ \mathbf{0} & \mathbf{0} & R \end{bmatrix} \tag{26}$$

and

$$\mathbf{M} = \begin{bmatrix} \mathbf{M}^{TT} & \mathbf{M}^{T\Phi} & \mathbf{m}^{Ti} \\ \mathbf{M}^{\Phi T} & \mathbf{M}^{\Phi\Phi} & \mathbf{m}^{\Phi i} \\ \mathbf{m}^{iT} & \mathbf{m}^{i\Phi} & m^{ii} \end{bmatrix} \tag{27}$$

where $\mathbf{x}^T$, $\mathbf{x}^\Phi$ are n_e- and n_n-vectors, respectively, $\mathbf{S}^{TT}$ and $\mathbf{M}^{TT}$ are n_exn_e matrices, and the dimensions of $\mathbf{M}^{T\Phi}$, $\mathbf{m}^{Ti}$, $\mathbf{M}^{\Phi T}$, $\mathbf{M}^{\Phi\Phi}$, $\mathbf{m}^{\Phi i}$, $\mathbf{m}^{iT}$ and $\mathbf{m}^{i\Phi}$ are n_exn_n, n_ex1, n_nxn_e, n_nxn_n, n_nx1, 1xn_e and 1xn_n, respectively. The elements of the sub-matrices are:

$$\mathbf{x}^T : \left\{ x_i^T(t) = t_i(t), \quad i = 1, 2, ..., n_e \right\}, \tag{28}$$

$$\mathbf{x}^\Phi : \left\{ x_i^\Phi(t) = \phi_i(t), \quad i = 1, 2, ..., n_n \right\}, \tag{29}$$

$$\mathbf{S}^{TT} : \left\{ \begin{array}{c} S_{ik}^{TT} = \int\limits_{\Omega_c} curl\mathbf{N}_i \cdot \frac{1}{\sigma} curl\mathbf{N}_k d\Omega, \\ i = 1, 2, ..., n_e, \quad k = 1, 2, ..., n_e \end{array} \right\}, \tag{30}$$

$$\mathbf{M}^{TT} : \left\{ \begin{array}{c} M_{ik}^{TT} = \int\limits_{\Omega_c} \mu \mathbf{N}_i \cdot \mathbf{N}_k d\Omega, \\ i = 1, 2, ..., n_e, \quad k = 1, 2, ..., n_e \end{array} \right\}, \tag{31}$$

$$\mathbf{M}^{T\Phi} : \left\{ \begin{array}{c} M_{ik}^{T\Phi} = -\int\limits_{\Omega_c} \mu \mathbf{N}_i \cdot gradN_k d\Omega, \\ i = 1, 2, ..., n_e, \quad k = 1, 2, ..., n_n \end{array} \right\}, \tag{32}$$

$$\mathbf{m}^{Ti} : \left\{ m_i^{Ti} = \int\limits_{\Omega_c} \mu \mathbf{N}_i \cdot \mathbf{t}_0 d\Omega, \quad i = 1, 2, ..., n_e \right\}, \tag{33}$$

$$\mathbf{M}^{\Phi T} : \left\{ \begin{array}{c} M_{ik}^{T\Phi} = -\int\limits_{\Omega_c} \mu gradN_i \cdot \mathbf{N}_k d\Omega, \\ i = 1, 2, ..., n_n, \quad k = 1, 2, ..., n_e \end{array} \right\}, \tag{34}$$

$$\mathbf{M}^{\Phi\Phi} : \left\{ \begin{array}{c} M_{ik}^{\Phi\Phi} = \int\limits_{\Omega_c + \Omega_n} \mu gradN_i \cdot gradN_k d\Omega, \\ i = 1, 2, ..., n_n, \quad k = 1, 2, ..., n_n \end{array} \right\}, \tag{35}$$

$$\mathbf{m}^{\Phi i} : \left\{ m_i^{Ti} = -\int\limits_{\Omega_c + \Omega_n} \mu gradN_i \cdot \mathbf{t}_0 d\Omega, \quad i = 1, 2, ..., n_n \right\}, \tag{36}$$

$$\mathbf{m}^{iT} : \left\{ m_k^{iT} = \int\limits_{\Omega_c} \mathbf{t}_0 \cdot \mu \mathbf{N}_k d\Omega, \quad k = 1, 2, ..., n_e \right\}, \tag{37}$$

$$\mathbf{m}^{i\Phi} : \left\{ m_k^{i\Phi} = -\int\limits_{\Omega_c + \Omega_n} \mathbf{t}_0 \cdot \mu gradN_k d\Omega, \quad k = 1, 2, ..., n_n \right\}, \tag{38}$$

$$m^{ii} = \int\limits_{\Omega_n + \Omega_c} \mathbf{t}_0 \cdot \mu \mathbf{t}_0 d\Omega. \tag{39}$$

The matrices **S** and **M** are symmetric, since, obviously, $\mathbf{S}^{TT}$, $\mathbf{M}^{TT}$ and $\mathbf{M}^{\Phi\Phi}$ are symmetric and $\mathbf{M}^{\Phi T}=(\mathbf{M}^{T\Phi})^{\mathrm{T}}$, $\mathbf{m}^{iT}=(\mathbf{m}^{Ti})^{\mathrm{T}}$, $\mathbf{m}^{i\Phi}=(\mathbf{m}^{\Phi i})^{\mathrm{T}}$ (the superscript T stands for transpose).

The unknown time function is now represented by a sequence of discrete time values at the time instants $t_k = t_{k-1} + \Delta t_k$, $k = 1, 2, ...$ Discretising (23) using the backward Euler difference scheme, one arrives at the nonlinear algebraic equation systems

$$\mathbf{S}\mathbf{x}_m + \frac{1}{\Delta t_m}\left[\mathbf{M}\left(\mu\left(\mathbf{x}_m\right)\right)\mathbf{x}_m - \mathbf{M}\left(\mu\left(\mathbf{x}_{m-1}\right)\right)\mathbf{x}_{m-1}\right] = \mathbf{f}_m, \quad m = 1, 2, ... \tag{40}$$

where the subscripts indicate time values, i.e. $\mathbf{x}_m = \mathbf{x}(t_m)$ and $\mathbf{f}_m = \mathbf{f}(t_m)$. Starting from $\mathbf{x}_0 = \mathbf{0}$, (40) is solved for $m = 1, 2, ...$ until the condition $\mathbf{x}(t_m) = \mathbf{x}(t_m+T)$ is satisfied with sufficient accuracy.

The equation systems (40) can be solved iteratively by re-computing the permeability at each Gaussian integration point in each iteration step from the previous approximation for $\mathbf{x}_m$. The iteration process is terminated once the variation of the permeability between two steps becomes small enough. Both the mean and the maximal value of the relative change over all integration points are monitored. In the *i*-th step, the modulus H_i of the magnetic field intensity is calculated from the approximation for $\mathbf{x}_m$ and B_{i+1} is derived from the *B-H* curve yielding the new permeability as B_{i+1}/H_i (see Fig. 2). This method is stable without introducing under-relaxation of the permeability provided the *B-H* curve is monotonous and convex (i.e. $dB/dH > 0$ and $d^2B/dH^2 < 0$) as it is the case for the curve in Fig. 2. The *B-H* curve of TEAM Problem No. 10 as defined in Table I is however concave ($d^2B/dH^2 > 0$) for low field values as in the domain $B<B_T$, $H<H_T$ in the curve shown in Fig. 3. In such a situation, the stability of the above secant method is no more ensured and it becomes necessary to use under-relaxation between the iteration steps. A slight modification, however, dispenses with the necessity of under-relaxation and thus results in an acceleration of convergence. In fact, the secant method remains stable in the concave domain, too if the value $B_i = \mu_i H_i$ is first computed with the aid of the old value μ_i of the permeability and the new field intensity H_{i+1} is hence obtained from the *B-H* curve. Thereupon, the new value μ_{i+1} of the permeability is derived as B_i/H_{i+1}.

It is noted here that, if a magnetic vector potential were used, i.e. the unknowns in $\mathbf{x}_m$ yielded the flux density instead of the magnetic field intensity, one would iterate the reluctivity $\nu=1/\mu$ instead of the permeability. In this case, the treatment of the convex part necessitates using the reluctivity from the previous iteration step: the vector potential values in $\mathbf{x}_m$ are used to compute the flux density B_i and this is multiplied by the reluctivity ν_i obtained in the previous step to yield the magnetic field intensity H_i. B_{i+1} is now obtained from the *B-H* curve and the new reluctivity ν_{i+1} is derived as the secant H_i/B_{i+1}. In the concave domain, the value of B_i is simply

obtained from $\mathbf{x}_m$ and H_{i+1} from the *B-H* curve to yield the new reluctivity ν_{i+1} as H_{i+1}/B_i. This is also illustrated in Figs 2 and 3.

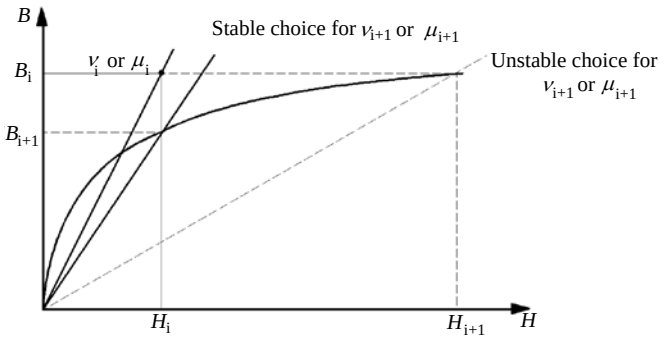

Fig. 2. Scheme of nonlinear iteration step for convex magnetizing curve

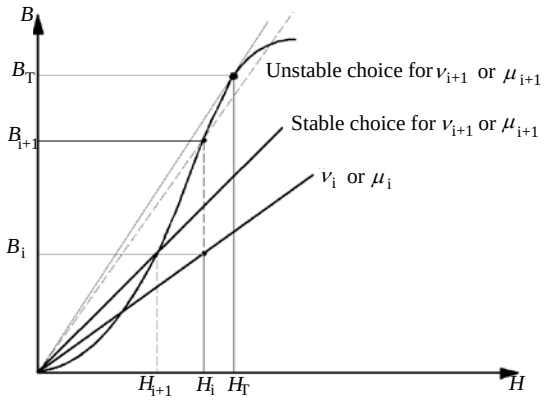

Fig. 3. Scheme of nonlinear iteration step for concave magnetizing curve

The secant method described here is superior to the more commonly used Newton-Raphson technique, since it does not necessitate the differentiation of the *B-H* curve to obtain differential permeabilities or reluctivities. This is especially advantageous, if the *B-H* curve is provided in discrete points instead of as a formula or a spline. In the experience of the authors, the convergence of the secant method is comparable to that of the Newton-Raphson approach, but it is insensitive to the initial guess for the permeability and is always stable.

B. Nonlinear time-harmonic method

A frequently used approximation to solve nonlinear eddy current problems with sinusoidal excitation is to assume that all field quantities also vary sinusoidally. This means that the time functions of the degrees of freedom for the vector potential and the scalar potential are assumed to be

$$t_k(t) = \hat{T}_k \cos\left(\omega t + \theta_k\right), \quad k = 1, 2, ..., n_e \tag{41}$$

and

$$\phi_k(t) = \hat{\Phi}_k \cos\left(\omega t + \varphi_k\right), \quad k = 1, 2, ..., n_n. \tag{42}$$

These can be transformed into the frequency domain, i.e. represented by their complex amplitudes (underlined in the following) as

$$\underline{\hat{T}}_k = \hat{T}_k e^{j\omega\theta_k}, \quad k = 1, 2, ..., n_e \tag{43}$$

and

$$\underline{\hat{\Phi}}_k = \hat{\Phi}_k e^{j\omega\varphi_k}, \quad k = 1, 2, ..., n_n \tag{44}$$

where j^2=-1. Hence, the complex amplitudes of the current vector potential and the magnetic scalar potential are

$$\underline{\hat{\mathbf{T}}}(\mathbf{r}) = \sum_{k=1}^{n_e} \underline{\hat{T}}_k \mathbf{N}_k(\mathbf{r}) \tag{45}$$

and

$$\underline{\hat{\Phi}}(\mathbf{r}) = \sum_{k=1}^{n_n} \underline{\hat{\Phi}}_k N_k(\mathbf{r}). \tag{46}$$

The vectors **x** and **f** are replaced by their complex amplitudes $\underline{\hat{\mathbf{X}}}$ and $\underline{\hat{\mathbf{F}}}$, respectively, whose elements are complex values:

$$\underline{\hat{\mathbf{X}}} = \begin{Bmatrix} \underline{\hat{\mathbf{X}}}^T \\ \underline{\hat{\mathbf{X}}}^\Phi \\ \underline{\hat{I}} \end{Bmatrix}, \tag{47}$$

$$\underline{\hat{\mathbf{F}}} = \begin{Bmatrix} \mathbf{0} \\ \mathbf{0} \\ \underline{\hat{U}} \end{Bmatrix}, \tag{48}$$

and

$$\underline{\hat{\mathbf{X}}}^T : \left\{ \underline{\hat{X}}_i^T = \underline{\hat{T}}_i, \quad i = 1, 2, ..., n_e \right\}, \tag{49}$$

$$\mathbf{X}^\Phi : \left\{ \underline{\hat{X}}_i^\Phi = \underline{\hat{\Phi}}_i, \quad i = 1, 2, ..., n_n \right\}. \tag{50}$$

$\underline{\hat{U}}$ is the given complex amplitude of the voltage and $\underline{\hat{I}}$ is the complex amplitude of the current to be determined.

Since the time derivative in the time domain corresponds to a multiplication by $j\omega$, (23) becomes a complex, nonlinear algebraic equation system:

$$\left[\mathbf{S} + j\omega\mathbf{M}\left(\mu\left(\underline{\hat{\mathbf{X}}}\right)\right)\right]\underline{\hat{\mathbf{X}}} = \underline{\hat{\mathbf{F}}}. \tag{51}$$

Several possibilities exist to choose the dependence of the permeability μ on the complex amplitude of the potentials (see e.g. [3]). In the present investigation, μ has been simply selected as the ratio of the maximal value of *B*(t) and *H*(t) over a period which have been assumed to be related to each other by the *B-H* curve in Table I.

The nonlinear complex algebraic equation system (51) can be solved using the nonlinear iterative method described in subsection A.

C. Time-domain fixed-point method

The periodicity condition can be ensured when using the backward Euler difference technique to discretise (23) by representing $\mathbf{x}(t)$ by a sequence of *N* equidistant time values within a period as $\mathbf{x}_k = \mathbf{x}(k\Delta t)$, $k = 0, 1, ..., N$ with Δt denoting the time step $\Delta t = T/N$. This sequence is cyclic, since due to the periodicity of **x**, we have $\mathbf{x}_0 = \mathbf{x}_N$. Therefore, (40) becomes

$$\mathbf{S}\mathbf{x}_m + \frac{1}{\Delta t}\left[\mathbf{M}\left(\mu\left(\mathbf{x}_m\right)\right)\mathbf{x}_m - \mathbf{M}\left(\mu\left(\mathbf{x}_{m-1}\right)\right)\mathbf{x}_{m-1}\right] = \mathbf{f}_m\,,$$
$$m = 1, 2, \ldots N \qquad (52)$$

where, as before, the subscripts indicate time values.

Let us introduce the notations

$$\mathbf{x}[1] = \left[\mathbf{x}_1 \quad \mathbf{x}_2 \quad \ldots \quad \mathbf{x}_N\right]^{\mathrm{T}}, \qquad (53)$$

$$\mathbf{x}[0] = \left[\mathbf{x}_0 \quad \mathbf{x}_1 \quad \ldots \quad \mathbf{x}_{N-1}\right]^{\mathrm{T}}, \qquad (54)$$

$$\mathbf{f}[1] = \left[\mathbf{f}_1 \quad \mathbf{f}_2 \quad \ldots \quad \mathbf{f}_N\right]^{\mathrm{T}} \qquad (55)$$

for the hyper-vectors formed by the cyclic sequences as well as

$$\langle\mathbf{S}\rangle = \begin{bmatrix} \mathbf{S} & \mathbf{0} & \ldots & \mathbf{0} \\ \mathbf{0} & \mathbf{S} & \ldots & \mathbf{0} \\ \ldots & \ldots & \ldots & \ldots \\ \mathbf{0} & \mathbf{0} & \ldots & \mathbf{S} \end{bmatrix}, \qquad (56)$$

$$\langle\mathbf{M}(\mu)\rangle = \begin{bmatrix} \mathbf{M}\left(\mu\left(\mathbf{x}_1\right)\right) & \mathbf{0} & \ldots & \mathbf{0} \\ \mathbf{0} & \mathbf{M}\left(\mu\left(\mathbf{x}_2\right)\right) & \ldots & \mathbf{0} \\ \ldots & \ldots & \ldots & \ldots \\ \mathbf{0} & \mathbf{0} & \ldots & \mathbf{M}\left(\mu\left(\mathbf{x}_N\right)\right) \end{bmatrix} \qquad (57)$$

for the block-diagonal matrices. Hence (52) can be written as

$$\left\langle\mathbf{S} + \frac{1}{\Delta t}\mathbf{M}[1](\mu)\right\rangle\mathbf{x}[1] - \frac{1}{\Delta t}\langle\mathbf{M}[0](\mu)\rangle\mathbf{x}[0] = \mathbf{f}[1]\,. \qquad (58)$$

Note that the matrices depending on the permeability vary in time. This is reflected in (58) by the symbols [1] and [0] following these matrices indicating the sampling operations defined in (53) and (54).

The discrete Fourier transform of the sequence **x**[1] is defined as [13]:

$$\hat{\mathbf{x}} = \mathcal{D}\left(\mathbf{x}[1]\right) = \left[\hat{\mathbf{x}}_1 \quad \hat{\mathbf{x}}_2 \quad \ldots \quad \hat{\mathbf{x}}_N\right]^{\mathrm{T}},$$
$$\hat{\mathbf{x}}_m = \mathcal{D}_m\left(\mathbf{x}[1]\right) = \sum_{k=1}^{N}\mathbf{x}_k e^{-j2\pi\cdot m\frac{k}{N}},\ m = 1, 2, \ldots N. \qquad (59)$$

This has the advantage that, according to the shift theorem [13], the discrete Fourier transform of **x**[0] can simply be obtained as

$$\mathcal{D}\left(\mathbf{x}[0]\right) = \mathbf{P}\hat{\mathbf{x}} \qquad (60)$$

where

$$\mathbf{P} = \begin{bmatrix} \mathbf{I}e^{-j2\pi\frac{1}{N}} & \mathbf{0} & \ldots & \mathbf{0} \\ \mathbf{0} & \mathbf{I}e^{-j2\pi\frac{2}{N}} & \ldots & \mathbf{0} \\ \ldots & \ldots & \ldots & \ldots \\ \mathbf{0} & \mathbf{0} & \ldots & \mathbf{I}e^{-j2\pi\frac{N}{N}} \end{bmatrix} \qquad (61)$$

and **I** is the unit matrix.

Applying the discrete Fourier transformation to (58), a system of equations with N times as many unknowns is obtained as there are elements, i.e. degrees of freedom, in $\mathbf{x}_k$:

$$\langle\mathbf{S}\rangle\hat{\mathbf{x}} + \frac{1}{\Delta t}\mathcal{D}\left\{\langle\mathbf{M}[1](\mu)\rangle\mathbf{x}[1] - \langle\mathbf{M}[0](\mu)\rangle\mathbf{x}[0]\right\} = \mathcal{D}\left(\mathbf{f}[1]\right) \qquad (62)$$

In the linear terms in (62), the elements of $\hat{\mathbf{x}}$, i.e. the discrete harmonics, are decoupled. Were it not for the dependence of **M** on μ, the shift in time would correspond to a multiplication by the block diagonal matrix **P**. The right hand side can be computed directly from **f**[1] as shown in (59). However, the nonlinear terms containing the permeability μ depending on the unknown solution couple all elements of the discrete Fourier transform, i.e. the discrete harmonics to each other. Therefore, due to the nonlinearity, one cannot solve for each discrete harmonic alone, a fact which, again, significantly increases the complexity of the problem.

Decoupling of harmonics

It is highly desirable that the discrete harmonics be decoupled and hence be determined independent of each other. This would lead to N systems of equations, each with as many unknowns as there are degrees of freedom in the FEM approximation. As shown below, the decoupling is trivial in the linear case but, for nonlinear problems, special techniques are needed.

Linear problems

If the permeability is independent of the magnetic field, the system of ordinary differential equations (23) becomes linear, since **M** does not depend on **x**(t). Hence, the discrete Fourier transform on the left hand side of (62) simplifies to

$$\mathcal{D}\left\{\langle\mathbf{M}(\mu)\rangle\mathbf{x}[1] - \langle\mathbf{M}(\mu)\rangle\mathbf{x}[0]\right\} = \langle\mathbf{M}(\mu)\rangle(\mathbf{I} - \mathbf{P})\hat{\mathbf{x}}\,. \qquad (63)$$

Therefore, the discrete harmonics in (62) are decoupled:

$$\left(\langle\mathbf{S}\rangle + \frac{1}{\Delta t}\langle\mathbf{M}(\mu)\rangle(\mathbf{I} - \mathbf{P})\right)\hat{\mathbf{x}} = \mathcal{D}\left(\mathbf{f}[1]\right). \qquad (64)$$

Indeed, these can be written as

$$\left[\mathbf{S} + \frac{1}{\Delta t}\mathbf{M}(\mu)\left(1 - e^{-j2\pi\frac{m}{N}}\right)\right]\hat{\mathbf{x}}_m = \mathcal{D}_m\left(\mathbf{f}[1]\right),\ m = 1, 2, \ldots N. \qquad (65)$$

Since the matrix **M** is real, the m-th and the (m+N/2)-th equations in (65) are complex conjugate to each other assuming N to be even, i.e. only N/2 linear systems have to be solved. The right hand side vector in (65) can be easily computed by discrete Fourier transformation as shown in

(59). If the excitation $\mathbf{f}(t)$ satisfies the condition $\mathbf{f}(t) = -\mathbf{f}(t+T/2)$ (this is the case if, e.g. it is a time-harmonic function), the right hand side of (65) and hence $\hat{\mathbf{x}}_m$ is zero for all even values of m, i.e. no more than $N/4$ linear systems have to be solved. Having obtained all vectors $\hat{\mathbf{x}}_m$ from (65), the time values can be obtained by inverse discrete Fourier transformation:

$$\mathcal{D}^{-1}(\hat{\mathbf{x}}) = \mathbf{x}[1] = \left[\mathbf{x}_1 \quad \mathbf{x}_2 \quad \ldots \quad \mathbf{x}_N\right]^{\mathrm{T}},$$
$$\mathbf{x}_m = \frac{1}{N}\sum_{k=1}^{N}\hat{\mathbf{x}}_k e^{j2\pi\cdot m\frac{k}{N}}, \quad m = 1, 2, \ldots N. \tag{66}$$

Fixed-point iteration technique for nonlinear problems

The fixed-point iteration method for the solution of nonlinear equations reduces the problem to finding the fixed point of a nonlinear function. The fixed point $\mathbf{x}_{FP}$ of the function $\mathbf{G}(\mathbf{x})$ is defined as

$$\mathbf{x}_{FP} = \mathbf{G}\left(\mathbf{x}_{FP}\right). \tag{67}$$

The fixed point can be determined as the limit of the sequence

$$\mathbf{x}^{(s+1)} = \mathbf{G}\left(\mathbf{x}^{(s)}\right), \quad s = 0, 1, 2, \ldots, \tag{68}$$

provided $\mathbf{G}(\mathbf{x})$ is a contraction, i.e. there exists a contraction number $0 < q < 1$ so that for any $\mathbf{x}$ and $\mathbf{y}$

$$\left\|\mathbf{G}(\mathbf{x}) - \mathbf{G}(\mathbf{y})\right\| \le q\left\|\mathbf{x} - \mathbf{y}\right\| \tag{69}$$

where $\|\cdot\|$ denotes a suitable norm. Furthermore, the sequence (68) converges to the same fixed point independent of the choice of the initial guess $\mathbf{x}^{(0)}$.

A general nonlinear equation $\mathbf{F}(\mathbf{x})=0$ can be transformed to a fixed-point problem by selecting a suitable linear operator $\mathbf{A}$ and defining $\mathbf{G}$ as

$$\mathbf{G}(\mathbf{x}) = \mathbf{x} + \mathbf{A}^{-1}\mathbf{F}(\mathbf{x}). \tag{70}$$

The fixed-point iterations (68) then become

$$\mathbf{A}^{(s)}\mathbf{x}^{(s+1)} = \mathbf{A}^{(s)}\mathbf{x}^{(s)} + \mathbf{F}\left(\mathbf{x}^{(s)}\right), \quad s = 0, 1, 2, \ldots \tag{71}$$

where the superscript s of $\mathbf{A}^{(s)}$ indicates that the linear operator $\mathbf{A}$ can be changed at each iteration step to accelerate convergence.

In case of the ordinary differential equations (23) obtained by Galerkin FEM techniques, the selection of a linear operator is straightforward: the permeability has to be set to a value independent of the magnetic field. This value μ_{FP} is not necessarily independent of the space coordinates $\boldsymbol{r}$, i.e. generally $\mu_{FP} = \mu_{FP}(\boldsymbol{r})$ is a permeability distribution varying in the problem domain but independent of the field and hence of time. By the same argument as the one used for the linear operator $\mathbf{A}$ above, μ_{FP} can also change at each iteration step. This fixed-point permeability function will be denoted by $\mu_{FP}^{(s)}$ below.

Once a suitable fixed-point permeability has been selected, (23) can be iteratively solved by obtaining $\mathbf{x}^{(s+1)}(t)$ from the equations

$$\mathbf{S}\mathbf{x}^{(s+1)}(t) + \frac{d}{dt}\left[\mathbf{M}\left(\mu_{FP}^{(s)}\right)\mathbf{x}^{(s+1)}(t)\right]$$
$$= \frac{d}{dt}\left[\mathbf{M}\left(\mu_{FP}^{(s)} - \mu^{(s)}\right)\mathbf{x}^{(s)}(t)\right] + \mathbf{f}(t), \quad s = 0, 1, 2, \ldots \tag{72}$$

at each step. The permeability distributions $\mu^{(s)}$ are determined from the solution $\mathbf{x}^{(s)}(t)$ i.e., in contrast to $\mu_{FP}^{(s)}$, they are time dependent. The mass matrix $\mathbf{M}$ on the right hand side of (72) is computed with $\mu_{FP}^{(s)} - \mu^{(s)}$ written instead of μ. This is permissible, since this matrix depends linearly on μ.

Since (72) is a linear ordinary differential equation system, it can be solved by the discrete Fourier decomposition method with decoupled harmonics. Indeed, the time discretised form of (72) is:

$$\left\langle\mathbf{S} + \frac{1}{\Delta t}\mathbf{M}\left(\mu_{FP}^{(s)}\right)\right\rangle\mathbf{x}^{(s+1)}[1] - \frac{1}{\Delta t}\left\langle\mathbf{M}\left(\mu_{FP}^{(s)}\right)\right\rangle\mathbf{x}^{(s+1)}[0]$$
$$= \frac{1}{\Delta t}\left[\left\langle\mathbf{M}[1]\left(\mu_{FP}^{(s)} - \mu^{(s)}\right)\right\rangle\mathbf{x}^{(s)}[1]\right.$$
$$\left. - \left\langle\mathbf{M}[0]\left(\mu_{FP}^{(s)} - \mu^{(s)}\right)\right\rangle\mathbf{x}^{(s)}[0]\right] + \mathbf{f}[1], s = 0, 1, 2, \ldots. \tag{73}$$

Taking the discrete Fourier transforms leads to equations similar to (65) for $s = 0, 1, 2, \ldots$:

$$\left[\mathbf{S} + \frac{1}{\Delta t}\mathbf{M}\left(\mu_{FP}^{(s)}\right)\left(1 - e^{-j2\pi\frac{m}{N}}\right)\right]\hat{\mathbf{x}}_m^{(s+1)}$$
$$= \frac{1}{\Delta t}\mathcal{D}_m\left[\left\langle\mathbf{M}[1]\left(\mu_{FP}^{(s)} - \mu^{(s)}\right)\right\rangle\mathbf{x}^{(s)}[1]\right.$$
$$\left. - \left\langle\mathbf{M}[0]\left(\mu_{FP}^{(s)} - \mu^{(s)}\right)\right\rangle\mathbf{x}^{(s)}[0] + \mathbf{f}[1]\right],$$
$$m = 1, 2, \ldots N \tag{74}$$

where $\mathbf{x}^{(s)}[1]$ is obtained from the discrete harmonics by inverse discrete Fourier transformation as shown in (66):

$$\mathbf{x}^{(s)}[1] = \left[\mathbf{x}_1^{(s)} \quad \mathbf{x}_2^{(s)} \quad \ldots \quad \mathbf{x}_N^{(s)}\right]^{\mathrm{T}},$$
$$\mathbf{x}_m^{(s)} = \frac{1}{N}\sum_{k=1}^{N}\hat{\mathbf{x}}_k^{(s)} e^{j2\pi\cdot m\frac{k}{N}}. \tag{75}$$

A time shift back yields $\mathbf{x}^{(s)}[0]$ according to the definition in (54).

The nonlinear iterations of solving the linear systems in (74) are terminated once the change of $\mu^{(s)}$ between two iteration steps becomes less than a suitable threshold. Similarly to the nonlinear iterations taken to solve (40), both the mean and the maximal value of the relative change over all integration points are monitored but, in addition, all time values within a period are swept. The most striking difference to the time-

stepping method is that, whereas there the time-stepping is the external loop with internal nonlinear iterations carried out, in case of the time-domain fixed-point method, the nonlinear iterations form the outer loop and time-stepping over one period is made internally.

The most computational effort is needed for the solution of the $N/2$ (or, e.g., in case of a time-harmonic excitation, $N/4$) linear equation systems in (74) (remember, half of the systems are complex conjugate to the other half). Since these are independent of each other, they can be solved parallel with each core responsible for the solution for one harmonic $\hat{\mathbf{x}}_m^{(s+1)}$. Once these parallel computations are ready, the right hand side for the next iteration can be determined by first computing the time function of the solution as in (75) and then carrying out the discrete Fourier decompositions indicated in (74). This is the part of the process when no parallelization is possible, but since the computational effort necessary for it is much less than needed to the solution of the large linear algebraic systems, the method is massively parallel.

One of the most important factors influencing the rate of the convergence of the fixed-point technique is the choice of the fixed-point permeability. As pointed out above, this is not necessarily constant with respect to the space coordinates, i.e. it can be selected to be different at each Gaussian integration point of the finite element mesh. The analysis of the optimal choice has been carried out in [8], the result for $\mu_{FP}^{(s)}$ below is taken from there:

$$\mu_{FP}^{(s)} = \max\left\{ \frac{\int_0^T \left[\mu^{(s)}\right]^2 dt}{\int_0^T \mu^{(s)} dt}, \frac{\min_{t\in[0,T]}\left(\mu^{(s)}\right) + \max_{t\in[0,T]}\left(\mu^{(s)}\right)}{2} \right\}. \quad (76)$$

The permeability $\mu^{(s)}$ is a function of the space coordinates and also of time since it is determined by the magnetic field distribution, itself space and time-dependent. According to (76), the fixed-point permeability depends on the space coordinates but not on time. The computational effort necessary for the evaluation of (76) in each nonlinear iteration step is negligible.

IV. Numerical results

The modified version of TEAM Problem No. 10 as defined in section II has been solved by the methods presented in the previous section.

A finite element model including of one eighth of the problem domain has been developed. The elements used are second order hexahedral ones with 20 nodes and 36 edges shown in Fig. 4 [14]. The discretization data are summarized in Table III.

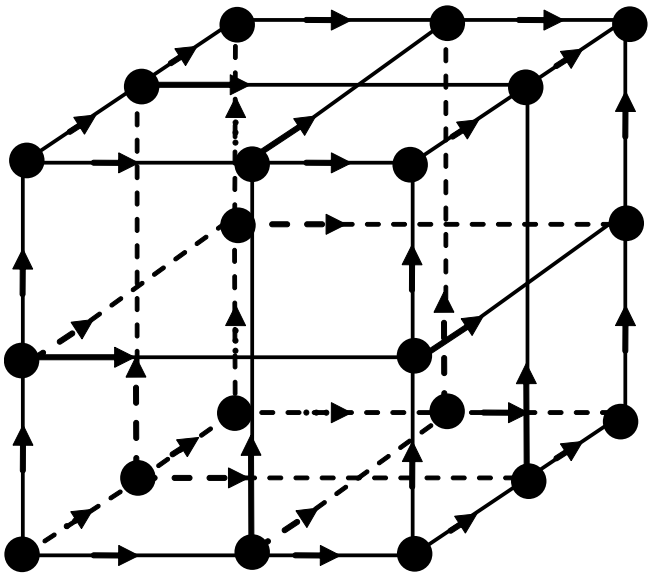

Fig. 4. A second order hexahedral element with 20 nodes and 36 edges

TABLE III. DISCRETISATION DATA OF THE FINITE ELEMENT MODEL

Number of elements	24,960
Number of nodes	107,893
Number of edges	315,444

The model is plotted in Fig. 5 with the finite element grid of the steel plates and the coil shown. As mentioned, it is sufficient to model one eighth of the problem region, since symmetry boundary conditions apply at $x = 0$ and $y = 0$ ($\mathbf{B}.\mathbf{n} = 0$) as well as at $z = 0$ ($\mathbf{H} \times \mathbf{n} = 0$). The finite element mesh extends in the three coordinate directions to a far boundary where the boundary condition $\mathbf{H} \times \mathbf{n} = 0$ is assumed. The coil is not modelled by the mesh.

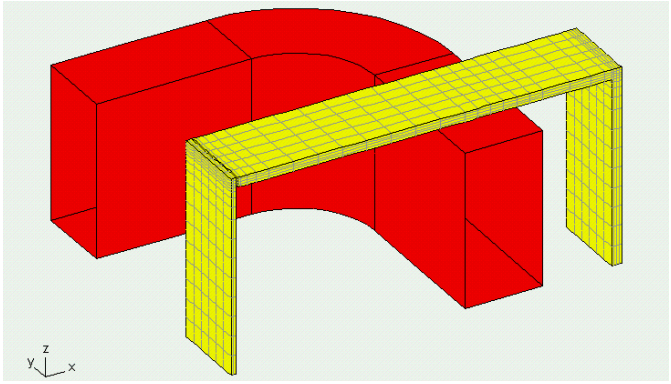

Fig. 5. Model of TEAM Problem No. 10

Applying the $\mathbf{T},\Phi$-Φ formulation described in section III.A, the number of degrees of freedom is 115,561 and the number of nonzeros in the upper triangle of the system matrix is 3,891,957.

A. Time-stepping method

The time-stepping method has been applied using a time-step of 0.5 *ms*, and 800 time-steps have been taken, i.e. 20 periods have been stepped through.

The nonlinear algebraic equation systems (40) have been solved in each time-step by the secant method presented. The linear algebraic equation systems arising at each nonlinear iteration step have been solved by the conjugate gradient method employing incomplete Cholesky preconditioning (ICCG). The initial guess for the ICCG method was the solution at the previous time-step for the first iteration within

a time-step and was chosen as the previous solution for the subsequent nonlinear iterations. The ICCG iterations were terminated as soon as the norm of the residual normalised by the norm of the right hand side had become less than 10^{-6}. The nonlinear iterations were stopped when the relative change of the permeability averaged over all Gaussian integration point had fallen below 1 percent and the maximal value of the relative change over all integration points had become less than 5 percent. In order to facilitate the comparison of the numerical efforts needed by the various methods, the total number of ICCG iterations carried out will also be shown for each analysis.

The computational data of the time-stepping method with 800 time-steps with the voltage amplitudes of 32 *V* and 64 *V* are shown in Table IV. The computations have been carried out on a single processor of a 16-core Intel Xeon E5-2687W server.

In case of the voltage amplitude being 32 *V*, the time function of the computed coil current is shown in Fig. 6. Increasing the voltage amplitude to 64 *V*, the time function plotted in Fig. 7 is obtained.

TABLE IV. COMPUTATIONAL DATA OF THE TIME-STEPPING METHOD

Voltage amplitude/*V*	32	64
Overall number of nonlinear iterations	10,869	13,101
Mean number of nonlinear iterations per time-step	13.6	16.4
Overall number of ICCG iterations	1,855,820	2,096,547
Mean number of ICCG iterations per nonlinear iteration	170.7	160.0
Overall CPU-time/*s*	130,661	147,610
CPU-time per ICCG iteration/*s*	0.0704	0.0704

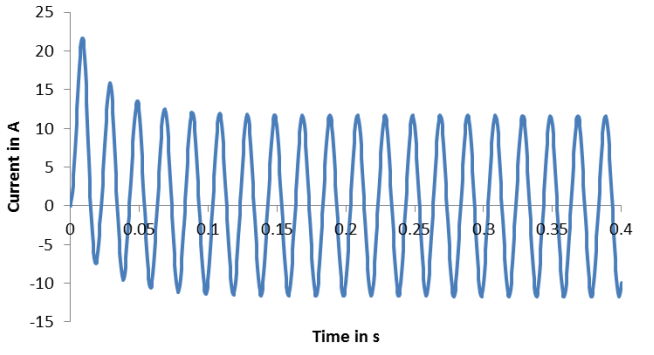

Fig. 6. Time function of coil current, voltage amplitude is 32 *V*

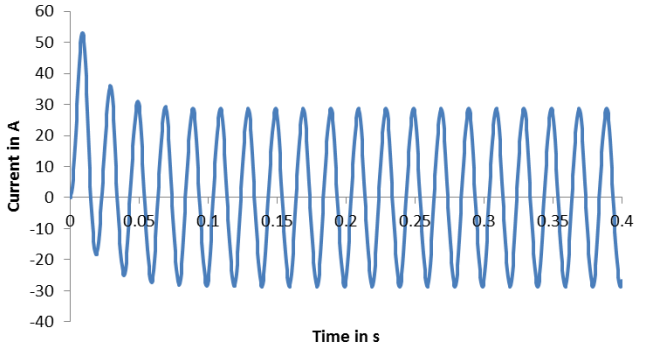

Fig. 7. Time function of coil current, voltage amplitude is 64 *V*

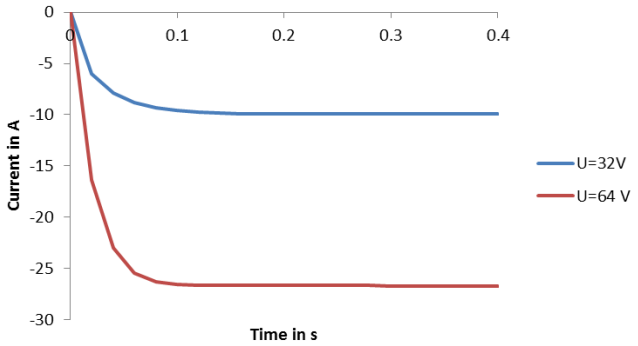

Fig. 8. Coil current values at the time instants $t = kT$, k =0, 1, ..., 20

To illustrate how the periodicity condition is satisfied for the 20 periods, Fig. 8 shows the current values at the time instant $t = kT$, k =0, 1, ..., 20 for both voltage values. It is obvious that the coil current has reached steady-state in the 20th period.

In addition to the coil current, the time evolution of the mean flux density B_1 in the centre of the middle plate and the power losses p in the steel plates have also been evaluated over the 20 periods. The mean flux density is shown in Figs. 9, 10 and 11 and the power losses in Figs. 12, 13 and 14.

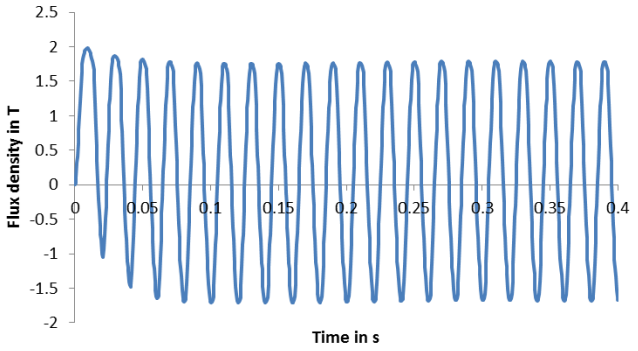

Fig. 9. Time function of mean flux density in the centre of the middle plate B_1, voltage amplitude is 32 *V*

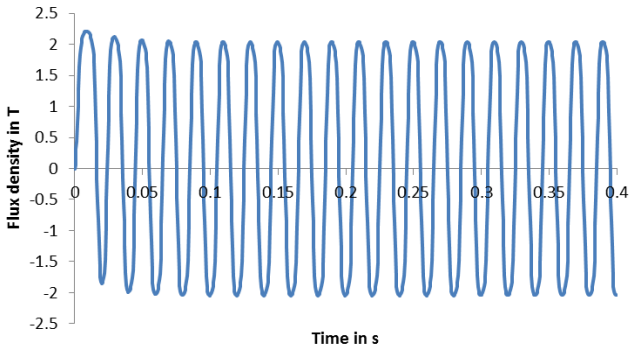

Fig. 10. Time function of mean flux density in the centre of the middle plate B_1, voltage amplitude is 64 *V*

It is clear that the mean flux density in the middle plate has already settled but the same is not true for the power losses, steady-state has been not yet arrived at, but the transients have been considerably damped.

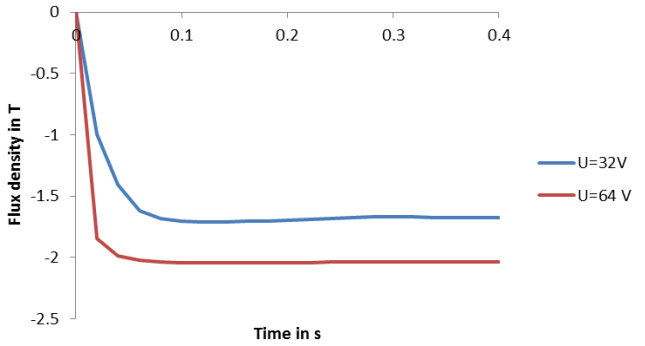

Fig. 11. Flux density values B_1 at the time instants $t = kT$, k =0, 1, ..., 20

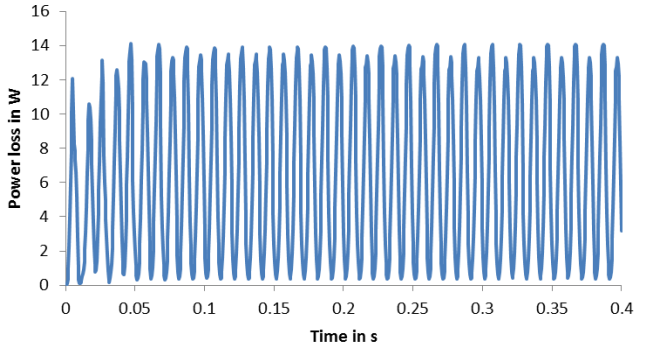

Fig. 12. Time function of power losses p in the plates, voltage amplitude is 32 V

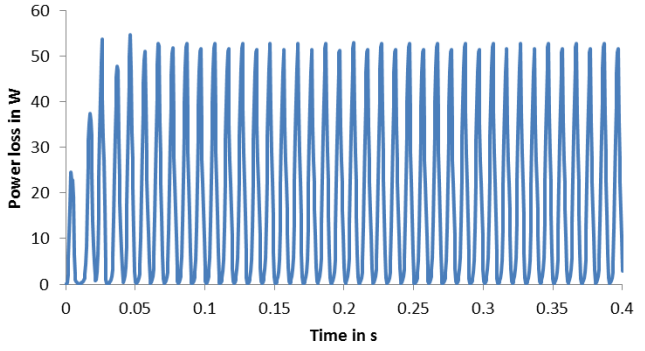

Fig. 13. Time function of power losses p in the plates, voltage amplitude is 64 V

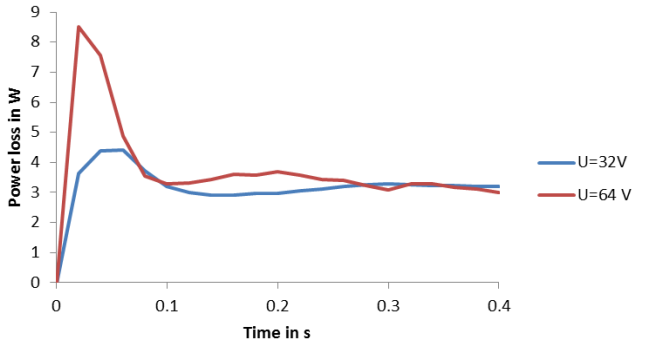

Fig. 14. Power loss values p at the time instants $t = kT$, k =0, 1, ..., 20

B. Nonlinear time-harmonic method

The computational data of the nonlinear time harmonic method are summarised in Table V. This approximate method is obviously much faster than the time-stepping approach.

TABLE V. COMPUTATIONAL DATA OF THE NONLINEAR TIME-HARMONIC METHOD

Voltage amplitude/V	32	64
Number of nonlinear iterations	18	21
Overall number of ICCG iterations	4,988	8,515
Mean number of ICCG iterations per nonlinear iteration	277.1	405.5
Overall CPU-time/s	349	581
CPU-time per ICCG iteration/s	0.0700	0.682

The sinusoidal time functions of the coil current and of the mean flux density in the centre of the middle plate as well as the time evolution of the power losses (being the sum of a constant value and a double frequency component) are compared in Figs. 15, 16 and 17 to the time functions obtained in the 20th period of the time-stepping method at the voltage amplitude of 32 V and in Figs. 18, 19 and 20 for the voltage amplitude of 64 V. The approximation is surprisingly good for the current and the flux density but much less satisfactory for the power losses.

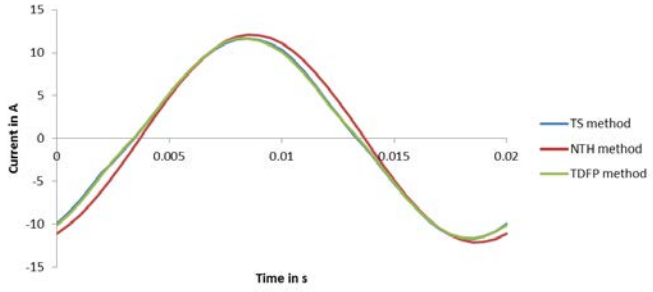

Fig. 15. Time function of the coil current in the 20th period computed by the time-stepping (*TS*) method, the sinusoidal time-function obtained by the nonlinear time-harmonic (*NTH*) approximation as well as the steady-state time evolution yielded by time-domain fixed-point (*TDFP*) technique, voltage amplitude is 32 V

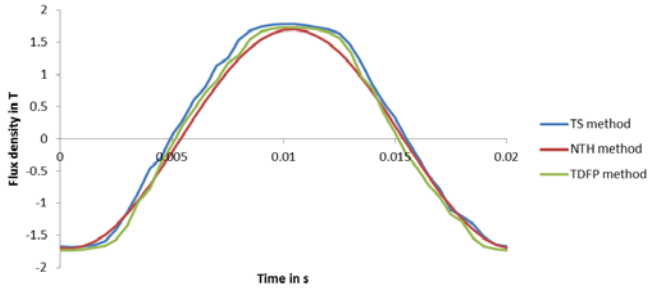

Fig. 16. Time function of the mean flux density in the centre of the middle plate in the 20th period computed by the time-stepping (*TS*) method, the sinusoidal time-function obtained by the nonlinear time-harmonic (*NTH*) approximation as well as the steady-state time evolution yielded by time-domain fixed-point (*TDFP*) technique, voltage amplitude is 32 V

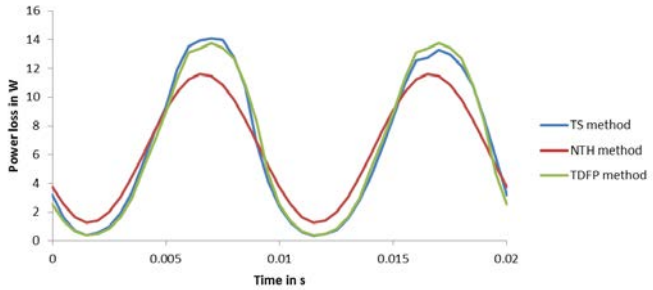

Fig. 17. Time function of the power losses in the plates in the 20th period computed by the time-stepping (*TS*) method, the sum of a constant value and of a double frequency sinusoidal time-function obtained by the nonlinear time-harmonic (*NTH*) approximation as well as the steady-state time evolution yielded by time-domain fixed-point (*TDFP*) technique, voltage amplitude is 32 V

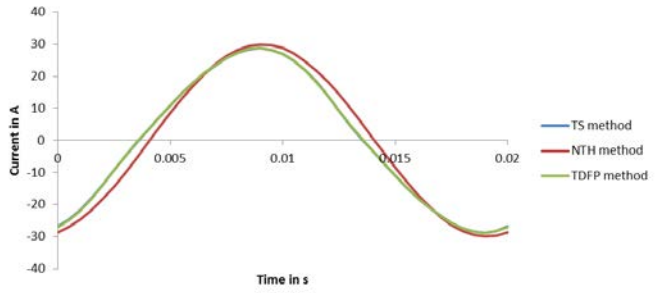

Fig. 18. Time function of the coil current in the 20th period computed by the time-stepping (*TS*) method, the sinusoidal time-function obtained by the nonlinear time-harmonic (*NTH*) approximation as well as steady-state the time evolution yielded by time-domain fixed-point (*TDFP*) technique, voltage amplitude is 64 *V*

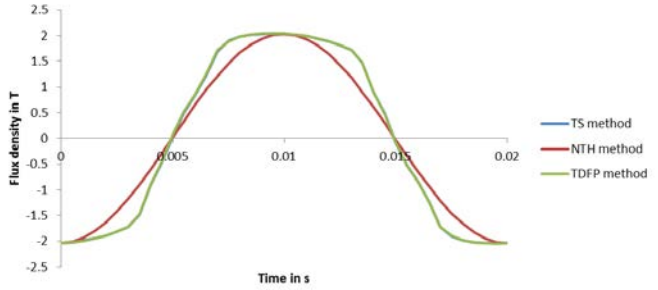

Fig. 19. Time function of the mean flux density in the centre of the middle plate in the 20th period computed by the time-stepping (*TS*) method, the sinusoidal time-function obtained by the nonlinear time-harmonic (*NTH*) approximation as well as the steady-state time evolution yielded by time-domain fixed-point (*TDFP*) technique, voltage amplitude is 64 *V*

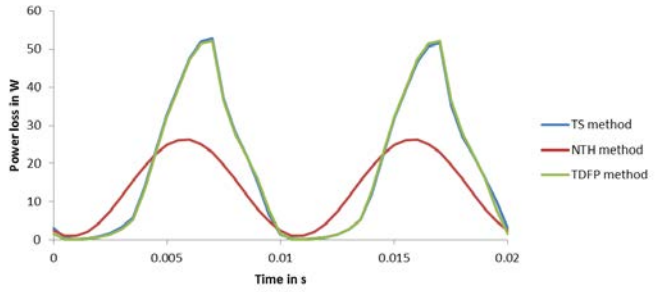

Fig. 20. Time function of the power losses in the plates in the 20th period computed by the time-stepping (*TS*) method, the sinusoidal time-function obtained by the nonlinear time-harmonic (*NTH*) approximation as well as the steady-state time evolution yielded by time-domain fixed-point (*TDFP*) technique, voltage amplitude is 64 *V*

C. Time-domain fixed-point method

Similarly to the time-stepping analysis, the time-step has been selected as 0.5 *ms* resulting in 40 time-steps per period. Due to the excitation being time-harmonic, this means that the number of independent linear equation systems (74) within each nonlinear iteration step is 10. Their solution has been carried out parallel. The thresholds for the ICCG iterations as well as for the termination of the nonlinear iterations have been selected to be the same as for the time-stepping method.

The computational data of the time-domain fixed-point method with the voltage amplitudes of 32 *V* and 64 *V* are shown in Table VI. The computations have been carried out on five processors of the 16-core Intel Xeon E5-2687W server used for the previous analyses.

TABLE VI. COMPUTATIONAL DATA OF THE TIME-DOMAIN FIXED-POINT METHOD

Voltage amplitude/*V*	32	64
Overall number of nonlinear iterations	46	86
Overall number of ICCG iterations	100,006	169,768
Mean number of ICCG iterations per nonlinear iteration per time step	217.4	197.4
Overall real time/*s*	2,843	5,233
Real time per ICCG iteration/*s*	0.0284	0.0308

The overall time needed is 28 to 46 times less than in case of the time-stepping method carried out for 20 periods. This factor could be considerably higher if the transients needed a longer time to fade, e.g. if the resistance of the coil were lower resulting in a larger time constant of the system. Indeed in such a case, the number of periods to be stepped through could be substantially higher than twenty; it could even be several thousand for a typical power transformer application.

The acceleration in comparison with the time-stepping method is not only due to the considerably lower number of ICCG iterations needed. Indeed, the CPU-time per ICCG iteration is also lower thanks to the parallelisation in solving the equation systems (74) within the nonlinear iteration steps. Note that the computation of the right hand side of (74) needs all the time values within the period, and this deteriorates the efficiency of the parallelisation: although five processors have been used, the time needed for one ICCG iteration is not less than about 40-45 percent of that of the nonparallelised time-stepping or nonlinear time-harmonic approaches (see Tables IV and V).

The computed steady-state time functions of the coil current, of the mean flux density in the centre of the middle plate as well as of the power losses in the plates have also been plotted in Figs. 15, 16, 17, 18 , 19 and 20. In case of the coil current and the flux density which have attained steady-state in the 20th period of the time-stepping, the time-domain fixed-point solutions are practically identical with these. The power losses have not yet settled in the 20th period as already seen in Fig. 14 and also clear in Fig. 17 showing that the two half periods are different. However, the time function of the power losses obtained by the time-domain fixed-point technique obviously satisfy the condition $p(t) = p(t+T/2)$.

The steady-state solutions obtained by the time-domain fixed-point method are illustrated by plots showing the moduli of the flux density and the current density in the plates at the time instants in which the mean flux density in the centre of the middle plate and the power losses attain their maximal value. Fig. 21 displays the flux density distribution in the plates at $t = 10.5$ *ms* with the voltage amplitude 32 *V*, and Fig. 22 presents the same for the voltage amplitude 64 *V*. The current density distribution at $t = 7$ *ms* is shown for 32 *V* in Fig. 23 and for 64 *V* in Fig. 24.

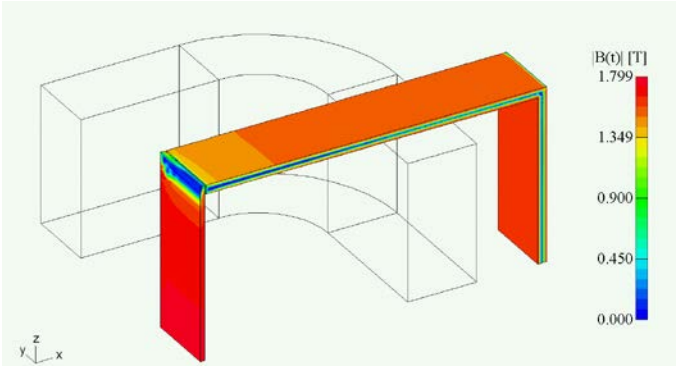

Fig. 21. Flux density distribution on the surface of the plates for the voltage amplitude 32 *V* at *t* = 10.5 *ms*

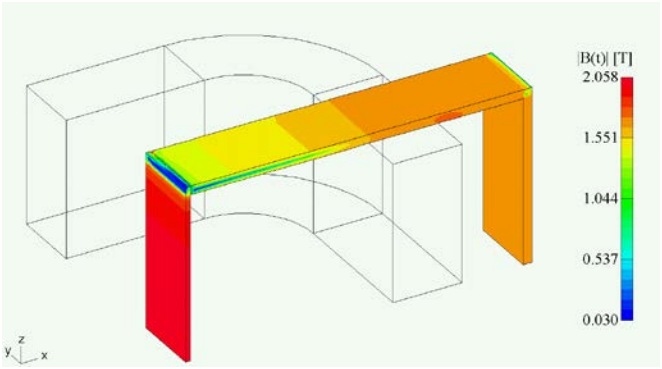

Fig. 22. Flux density distribution on the surface of the plates for the voltage amplitude 64 *V* at *t* = 7.0 *ms*

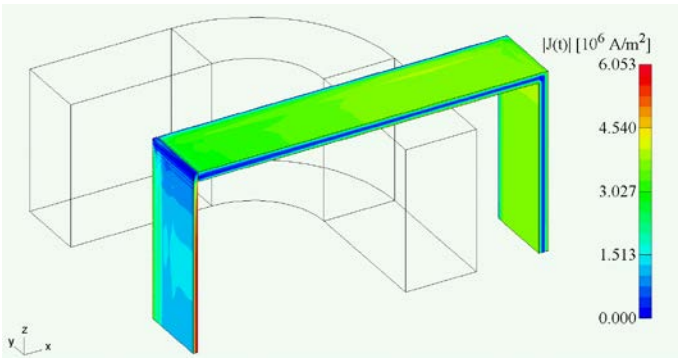

Fig. 23. Current density distribution on the surface of the plates for the voltage amplitude 32 *V* at *t* = 7.0 *ms*

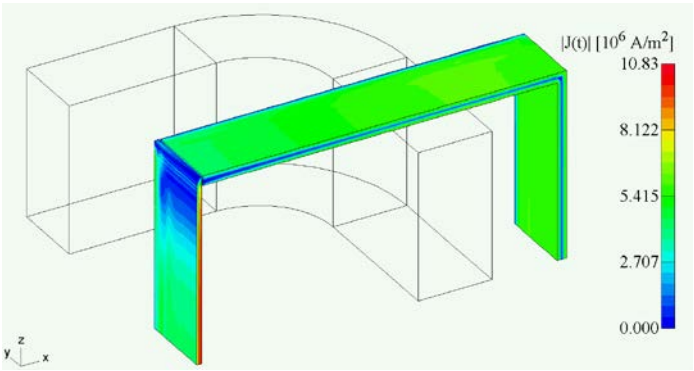

Fig. 24. Current density distribution on the surface of the plates for the voltage amplitude 64 *V* at *t* = 7.0 *ms*

V. Conclusion

The solutions presented for TEAM Workshop Problem No. 10 with a sinusoidal voltage excitation have illustrated that the time-domain fixed-point method can efficiently compute the steady-state of nonlinear eddy current problems roughly at the expense of time-stepping through one period.

VI. References

[1] Albanese, R., Coccorese, E., Martone, R., Miano, G., Rubinacci, G., "Periodic solutions of nonlinear eddy current problems in three-dimensional geometries", *IEEE Trans. Magn.* 28, 1992, 1118-1121.

[2] Lavers, J. D., "Finite element solution of nonlinear two dimensional TE- mode eddy current problems," *IEEE Trans Magn.* 19, 1983, 2201-2203.

[3] Paoli, G., Bíró, O., Buchgraber, G., "Complex representation in nonlinear time harmonic eddy current problems," *IEEE Trans Magn.* 34, 1998, 2625-2628.

[4] Hara, T., Naito, T., Umoto, J., "Time-periodic finite element method for nonlinear diffusion equations", *IEEE Trans. Magn.* 21, 1985, 2261-2264.

[5] Takahashi, Y., Tokumasu, T., Kameari, A., Kaimori, H., Fujita, M., Iwashita, T., Wakao S., "Convergence acceleration of time-periodic electromagnetic field analysis by the singularity decomposition-explicit error correction method", *IEEE Trans. Magn.* 46, 2010, 2947-2950.

[6] Takahashi, Y., Iwashita, T., Nakashima, H., Tokumasu, T., Fujita, M., Wakao, S., Fujiwara, K., Ishihara, Y., "Parallel time-periodic finite-element method for steady-state analysis of rotating machines", *IEEE Trans. Magn.* 48, 2012, 1019-1022.

[7] Bíró, O., Preis, K., "An efficient time domain method for nonlinear periodic eddy current problems", *IEEE Trans. Magn*. 42, 2006, 695–698.

[8] Koczka, G., Ausserhofer, S., Bíró, O., Preis, K., "Optimal convergence of the fixed-point method for nonlinear eddy current problems", *IEEE Trans. Magn.* 45, 2009, 948-951.

[9] Bíró, O., Koczka, G., Preis K., "Finite element solution of nonlinear eddy current problems with periodic excitation and its industrial applications", *Appl. Num. Math.* 79, 2014, 3-17.

[10] Nakata, T., Fujiwara, K. "Results for benchmark problem 10 (steel plates around a coil)", *COMPEL* 9, 1995, 181-190.

[11] Turner, L. ed., *TEAM Workshops, Test Problems*, Fusion Power Program, Argonne National Lab., USA, 1988.

[12] Nakata, T., Takahashi N., Fujiwara, K., Okada, Y., "Improvements of the **T**-Ω method for 3-D eddy current analysis", *IEEE Trans. Magn.* 24, 1988, 94-97.

[13] Brigham, E. O., The fast Fourier transform and its applications. Englewood Cliffs, N.J., Prentice Hall, 1988.

[14] Kameari, A., "Calculation of transient 3D eddy current using edge-elements", *IEEE Trans. Magn.* 24, 1990, 118-121.

Authors Name and Affiliation

Oszkár Bíró, IGTE, Graz University of Technology, Inffeldgasse 18, A-8010 Graz, Austria, +43 316 873 7263, biro@tugraz.at

Gergely Koczka, Siemens Inc. Austria – Transformers Weiz, A-8160 Weiz, Austria, gergely.koczka@siemens.com

Kurt Preis, IGTE, Graz University of Technology, Inffeldgasse 18, A-8010 Graz, Austria, +43 316 873 7264, kurt.preis@tugraz.at